

**NASA TECHNICAL  
MEMORANDUM**

**N 71 - 3 6 8 1 5**  
NASA TM X- 67949

NASA TM X- 67949

**DESIGN FEATURES AND RESULTS FROM FATIGUE  
RELIABILITY RESEARCH MACHINES**

by Vincent R. Lalli, Dimitri Kececioglu,  
and Jeffrey B. McConnell  
Lewis Research Center  
Cleveland, Ohio

TECHNICAL PAPER prepared for presentation at  
1971 Fall Meeting of the Society for  
Experimental Stress Analysis  
Milwaukee, Wisconsin, October 19-22, 1971

# DESIGN FEATURES AND RESULTS FROM FATIGUE

## RELIABILITY RESEARCH MACHINES

The design, fabrication, development, operation, calibration and results from reversed bending combined with steady torque fatigue research machines are discussed<sup>1</sup>

by Vincent R. Lalli, Dimitri Kececioglu,  
and Jeffrey B. McConnell\*

Lewis Research Center  
National Aeronautics and Space Administration  
Cleveland, Ohio

### ABSTRACT

The design, fabrication, development, operation, calibration and results from reversed bending combined with steady torque fatigue research machines are presented. Fifteen-centimeter long, notched, SAE 4340 steel specimens are subjected to various combinations of these stresses and cycled to failure. Failure occurs when the crack in the notch passes through the specimen automatically shutting down the test

---

\* Vincent R. Lalli is Head of Environmental Laboratory, Spacecraft Technology Division, NASA-Lewis Research Center, Cleveland, Ohio. Dr. Dimitri Kececioglu is Professor of Aerospace and Mechanical Engineering, The University of Arizona, Tucson, Arizona. Jeffrey B. McConnell is a Member of the Technical Staff, Tucson Engineering Lab, Huges Aircraft Co., Tucson, Arizona.

<sup>1</sup>This paper is based on research conducted for the National Aeronautics and Space Administration, Lewis Research Center, Cleveland, Ohio, under Grant No. NGR-03-002-044. Inquiries concerning this innovation may be directed to: Technology Utilization Office, Lewis Research Center, 21000 Brookpark Road, Cleveland, Ohio, 44135.

machine. These cycles-to-failure data are statistically analyzed to develop a probabilistic S-N diagram. These diagrams have many uses; a rotating component design example given in the literature shows that minimum size and weight for a specified number of cycles and reliability can be calculated using these diagrams.

### SYMBOLS

C	specimen radius, cm
d	specimen groove diameter, cm
E	Young's modulus, Gg/m <sup>2</sup>
G	gage factor
I	moment of inertia, m <sup>4</sup>
J	polar moment of inertia, m <sup>4</sup>
K <sub>BGR, B/T, BTH, GRTH, T, T/B</sub>	coefficients: BGR, bending in groove; B/T, bending interaction into torque; BTH, bending to toolholder; GRTH, groove to toolholder; T, toolholder torque; T/B, torque interaction into bending
K <sub>a→f, t, f</sub>	factors: a→f, modifying; t, stress concentration; f, miscellaneous effects
M	bending moment on specimen, m-kg
N <sub>a, c, v</sub>	coefficients: a, number active arms strain bridge; c, visicorder divisions; v, visicorder
R <sub>1→4, c, g</sub>	coefficients: 1→4 gage resistance, ohms; c, calibration resistance, ohms; g, equivalent gage resistance, ohms
r <sub>s</sub>	stress ratio, s <sub>a</sub> /s <sub>m</sub>

$S_{a, m}$	probabilistic Goodman diagram material strength, $Mg/m^2$ ; a, alternating; m, mean
$S_e$	corrected endurance limit, $Mg/m^2$
$S'_e$	estimated endurance limit of rotating beam specimen, $Mg/m^2$
T	torque on specimen, kg-m
$\sigma_{x, a, c, m, n, o, t}$	bending stress, $Gg/m^2$ : a, alternating; c, compression; m, mean; n, notch; o, output; t, tension
$\tau_{xy, a, m, n, o}$	shear stress, $Gg/m^2$ : a, alternating; m, mean; n, notch; o, output

## INTRODUCTION

Combining reversed bending with steady torque for fatigue testing of metal specimens was previously discussed by Mabie and Gjesdahl in an SESA paper (1).<sup>2</sup> This paper explained a test machine using the four-square and rotating-beam principles. The four square principle couples torque to a specimen through a connecting shaft, two end gear boxes and a second shaft for torque loading. The rotating beam principle applies reverse bending through bearings and a static fixed force. These basic methods of applying combined stresses to metal test specimens without the need to dissipate energy proved satisfactory. However, this first machine was not able to hold torque or bending stresses constant and developed excessive noise and vibration during operation.

Probabilistic design applied to space power system shafts required that a test machine capable of providing this environment for metal specimens be developed (2). Using the proven principles of the Mabie-Gjesdahl machine, The University of Arizona set out to conceive, design and build a

---

<sup>2</sup>Numbers in brackets in the written text pertain to references in bibliography at end of paper.

test machine to obtain data to support this design need. The proposed test machine was carefully reviewed, modified where appropriate and approved for manufacturing by the NASA Lewis Research Center. This paper describes the test machine resulting from these efforts.

## THE TEST MACHINE

The fatigue machine consists of a two-section, rotating shaft in the front with a test specimen locked in the center, as shown in figure 1. The front shaft has a flexible coupling<sup>3</sup> at each end to allow for relatively free deflection when the specimen is loaded. A direct drive 200 watt (7.5 hp), 1800 rpm motor powers the front shaft. The bending load is applied to the specimen by means of two yokes, one on each of two bearings located symmetrically about the specimen on two commercial tool holders. Below the shaft, the yokes are connected by a horizontal link, which concentrates the load at a single vertical link in the center. The vertical link is then connected to either a long or a short loading lever arm. These loading arms make possible the application of a range of bending stresses in the specimen groove, by means of pan weights applied at the end of the loading arm. One kilogram (1 lb) of pan weight is equal to approximately  $140 \text{ Mg/m}^2$  bending (2 kpsi) stress in the groove. The torque is applied by means of a commercial, Infinit-Indexer which is located on the back shaft of the machine rotating at about 1000 rpm. Table I summarizes the operational specifications for this research machine. The machine is capable of producing,

---

<sup>3</sup>The original front shaft coupling design is shown in figure 2(a). This design had to be changed because radial shear load caused the sleeve to cock allowing the centerline of one shaft to fall below the centerline of the other; this caused vibration, rapid wear and pivot point variations. The coupling was redesigned, see figure 2(b), to correct for these deficiencies by adding a spherical bearing to absorb the radial shear loads and create a definite point about which the toolholder arms can pivot (3).

holding and transmitting to the rotating specimen steady torques of up to 62 m-kg (5400 lb-in.) and reversed bending moments of up to 40 kg-m (3450 in.-lb). Specimens of diameters up to 2.5 centimeters (1 in.) can be tested in this machine by changing the collets in the specimen holder.

### THE TEST SPECIMEN

Typical space power turbine shaft designs were analyzed to make the research data directly applicable to aerospace problems. Figure 3 shows the grooved test specimen details. Bar stock pieces 15 centimeters (6 in.) long were carefully machined to the dimensions and finish specified in figure 3(a). The reverse bending moment,  $M$ , torque,  $T$ , bending stress,  $\sigma_{xa}$ , and shear stress,  $\tau_{xym}$ , are also defined in this figure.

Each specimen is installed in the test machine and the instrumentation is checked for zero adjustment and calibration. The appropriate bending moment is applied to the specimen by putting weights on the load pan. The torque is applied to the specimen by rotating the outer shell of the Infinit-Indexer with a suitable wrench. The timing clock is set to zero and the machine is started. When the specimen fractures a micro-switch stops the clock and the machine. Figures 3 and 4 show the specimen configuration and fracture pattern after testing.

### THE TEST INSTRUMENTATION

Strain gages are used on the toolholder to monitor the bending and torque loads. These gages are located on the toolholder directly behind the collets rather than on the specimen groove. The reasons for this are: (1) it is extremely difficult to mount strain gages in the limited space of the specimen groove; and (2) since the specimens are not reusable, the gages could also be damaged during failure resulting in prohibitive expenses. The positioning and electrical circuitry for the strain gage bridges are given in figure 5. The double-gages are mounted  $90^{\circ}$  apart in one piece on the toolholder surface so that the two gages make an angle of  $45^{\circ}$  with the toolholder axis of rotation. Table II contains the specifications for the instrumentation

components. The slip-ring assembly is located adjacent to the strain gages. The slip-rings are counterbalanced with an aluminum collar of equal weight and nearly equal dimensions located on the other toolholder, as shown in figure 1. The amplifiers, galvanometers and recorder are matched units. This equipment is used to amplify and record the output from the bending and torque gages.

## CALIBRATION

Measurement of the nominal bending and shear stresses in the specimen groove are required for the Probabilistic Design Methodology. Since the strain gages cannot be located in the specimen groove, the shear and bending stresses in the specimen groove must be determined from the collet assembly strain gage signals. To convert collet assembly data to specimen groove stresses, the following calibration procedure was worked out:

1. Selected groove bending stress to produce apparent groove bending stress.
2. Apparent groove bending stress to produce apparent toolholder bending stress.
3. Torque interaction into bending.
4. Selected groove shear stress to produce toolholder shear stress.
5. Bending interaction into torque.

Each machine was carefully calibrated. The relation between the calibration variables, in each case, proved to be linear, hence a slope could be associated with each calibration variable. Since for all cases, the functional relation began at the origin, the slope alone of each curve completely defined the function. These slopes have been given calibration coefficient designations and are listed in table III. The mode of use of the calibration results is described in detail in figure 6. Steps 1 and 2 require the selection of a stress ratio and a bending stress level. The nominal shear stress in the specimen groove to give this ratio is found in Step 3. Next, in Step 4, the nominal bending stress in the groove is converted to output stress in the groove using  $K_{BGR}$  and  $K_{GRTH}$ . Figure 5 also shows the laboratory

setup used to obtain these bending coefficients. On the torque side, Step 5 gives the equation for converting the nominal shear stress in the groove to shear stress in the toolholder. Also, in Step 5, the shear stress in the toolholder is converted to output stress. Figure 7 shows the laboratory setup used to obtain the torque coefficients. Steps 6 and 7 are the corrections for interaction between torque and bending. Steps 8 and 9 convert the corrected output stress to visicorder divisions, completing the procedure.

The machine has the following calibration equation for bending (B):

$$N_{vB} = \frac{N_c N_a GR_c}{ER_g} (K_{BGR} K_{GRTH} \bar{\sigma}_n + K_{T/B} \bar{\tau}_{OTH}), \quad (1)$$

and for torque (T),

$$N_{vT} = \frac{N_c N_a GR_c}{ER_g} \left( \frac{K_{BTH}}{K_T} \bar{\tau}_n + K_{B/T} \bar{\sigma}_{OTH} \right). \quad (2)$$

All strain gage parameters being those of the bending and torque bridges, respectively.

### TEST DATA REDUCTION

The recorded test data is presently being reduced for use in the Probabilistic Design Methodology by a combination of manual and digital computer techniques. Planned improvements in this data reduction method will make use of an on site analog computer. Efforts thus far have been restricted to obtaining data necessary to design rotating shafts. Additional work on four other types of test machines to get more probabilistic design data has also been started (4).

Briefly the theory and equations necessary for data reduction are summarized in the next few paragraphs. The probabilistic<sup>4</sup> stress ratio is

---

<sup>4</sup>These are random variables defined by statistical functions and the indicated mathematical operations are performed using suitable statistical methods.

defined as the quotient of the alternating bending stress to the mean shear stress and is given by

$$\text{Stress ratio} = r_s = \frac{s_{\text{alternating}}}{s_{\text{mean}}} = \frac{\sigma_{xa}}{\sqrt{3} \tau_m} \quad (3)$$

where  $\sqrt{3}$  is a constant resulting from the use of the von Mises-Hencky failure criterion (5, p. 50). According to the von Mises-Hencky criterion (6, p. 154), the failure governing alternating stress,  $s_a$ , in fatigue is given by

$$s_a = \sqrt{\sigma_{xa}^2 - \sigma_{xa}\sigma_{ya} + \sigma_{ya}^2 + 3\tau_{xza}^2} \quad (4)$$

and the failure governing mean stress,  $s_m$ , by

$$s_m = \sqrt{\sigma_{xm}^2 - \sigma_{xm}\sigma_{ym} + \sigma_{ym}^2 + 3\tau_{xzm}^2}$$

For the specimen geometry and loads used in this research the following conditions apply:

$$\sigma_{ya} = \tau_{xza} = 0$$

$$\sigma_{xm} = \sigma_{ym} = 0$$

Consequently, equations (4) and (5) reduce to

$$s_a = \sigma_{xa} = \frac{Mc}{I} \quad (6)$$

$$s_m = \sqrt{3} \tau_m = \sqrt{3} \frac{Tc}{J} \quad (7)$$

Substituting the proper values in equations (6) and (7) gives

$$s_a = \frac{Md/2}{\pi d^4/64} = 10.2 \frac{M}{d^3} \quad (8)$$

$$s_m = \sqrt{3} \frac{Td/2}{\pi d^4/32} = 8.82 \frac{T}{d^3} \quad (9)$$

For data reduction, first, a stress ratio and a bending stress level in the groove are selected, as shown in blocks 1 and 2 of figure 6. From these two parameters, the nominal shear stress in the groove is determined in block 3. This step employs the von Mises-Hencky failure criterion. Next, the nominal bending stress in the groove is converted to collet assembly stress in block 4. In block 5, the theoretical conversion from the groove to toolholder torque and from nominal to output toolholder stress is made for shear. It is not true that the bending moment applied to the groove is the same as that applied to the toolholder. In blocks 6 and 7, each toolholder output is corrected for interaction effects. In blocks 8 and 9, the output toolholder stresses are converted to recorder divisions. Thus, the number of recorder divisions necessary to give the required stress ratio and bending stress level are determined.

Next, a sample of eighteen specimens is run, maintaining the necessary divisions of bending and torque as closely as possible. A record of the bending and torsion gage signals is taken for every specimen. A sample of a fatigue test record including data reduction lines is given in figure 8. The variation in the torque bridge output is due to the interaction of bending load into the torque bridge output. When the running of the sample lot is complete, the data reduction procedure is reversed for each specimen to determine the nominal bending and shear stresses and the stress ratio achieved.

## TEST RESULTS

When a specimen is subjected to an alternating stress, at stress levels near the endurance strength, cracks will form and propagate to cause fracture or fatigue failure. If the same level of alternating stress is applied to several specimens, the scatter in the number of cycles necessary to produce fatigue failure is quite large. This scatter exceeds experimental error, and the statistical nature of this scatter has been recognized. This scatter is now considered to be a fundamental characteristic of fatigue data and should be considered in any fatigue analysis.

Mechanical components with sharp changes in section without adequate fillets tend to concentrate stresses encountered in service and promote failure in progressive fracture. Several factors are known to have pronounced effect on fatigue failures: design, composition, material flaws, residual stresses, and loading. Examining fractured surfaces enables the investigator to determine if certain conditions existed in dynamically stressed parts. Fracture analysis is a valuable tool in the determination of the causes of a fatigue fracture. It is possible, for example, to determine the presence of an inadvertently introduced stress concentration in the part. Fracture surface data to differentiate between types of bending or torsional loads are given in the literature (4, 7, 8). Figure 4 shows a close-up photograph of the fractured notch section of two specimens. Figure 4(a) is for a mean bending stress,  $\sigma_{xa}$ , of 80 Gg/m<sup>2</sup> (114 kpsi) and a mean shear stress,  $\tau_{xym}$ , of zero, i. e., no torque was applied to the test specimen through the Infnit-Indexer, and figure 4(b) is for a mean bending stress of 78 Mg/m<sup>2</sup> (111 kpsi) and a mean shear stress of 54 Mg/m<sup>2</sup> (77.3 kpsi). The dark central portion shows the section supporting the loads just prior to complete fracture. The light portion shows how the crack grows with fatigue. A study of such fracture patterns may reveal the magnitude and types of loads which caused the failure. Such a study will be conducted in Phase II of this research.

A typical probabilistic S-N diagram is given in figure 9. Figure 9 shows the cycles-to-failure distributions and the endurance strength distribution for a stress ratio of  $\infty$ , or for zero mean shear stress. An analysis of the cycles-to-failure data shows the distributions are lognormally distributed and therefore plot as normal distribution on logarithmic graph paper (9).

The endurance tests were conducted using the staircase method. In the staircase method, the bending stress is changed in increments of  $2.11 \text{ Gg/m}^2$  (3.0 kpsi) while maintaining a constant stress ratio. If there is no failure during a 2.5 million cycle test, then another increment is added to the bending stress level and the test repeated. If a failure occurs one increment is subtracted.

The mean value of the S-N diagram of figure 9 and a theoretical S-N diagram for various ratios, are plotted in figure 10 for purposes of comparison. The theoretical S-N diagram was constructed according to the procedure recommended by Shigley (6, p. 162).

The fatigue strength of the specimen,  $S_e$ , at  $10^3$  cycles  $= 0.9 S_U$ ,

$$S_U = 125 \text{ Gg/m}^2 \text{ (178 kpsi) for unnotched specimens,}$$

$$S_{e_{10^3}} = 0.9 \times 125 \text{ (178)}; \text{ hence,}$$

$$S_{e_{10^3}} = 112 \text{ Gg/m}^2 \text{ (160 kpsi)}$$

The endurance strength is given by (6, p. 166)

$$S_e = k_a k_b k_c k_d k_e k_f S'_e \quad (10)$$

For the specimens used in this research according to Shigley's data

$k_a$  = surface finish factor = 0.89, for ground finish

$k_b$  = size factor = 0.85, for  $D \leq 5.0 \text{ cm}$  (2.0 in.) in bending

$k_c$  = not used (2)

$k_d$  = temperature factor = 1.0, not temperature effect

$k_e$  = stress concentration design factor =  $1/K_f$

$$k_f = 1 + q(K_t - 1)$$

$$q = 0.92$$

$$K_t = 1.45, \text{ obtained from Peterson's data (10)}$$

Hence,

$$K_f = 1 + 0.92(1.45 - 1),$$

$$K_f = 1.41, \text{ and } k_f = 1/K_f = 1/1.41 = 0.709$$

$$k_f = \text{miscellaneous effects factor} = 1.$$

$$S'_e = 0.5 S_U \text{ (6, p. 162)}$$

Therefore,

$$S'_e = 0.5 \times 125 (178) = 65.5 \text{ Gg/m}^2 \text{ (89 kpsi)}$$

Using equation (8)

$$S_e = (0.89)(0.85)(1.0)(0.709)(1.0)(6.55) = 33.5 \text{ Gg/m}^2 \text{ (47.4 kpsi)}$$

Figure 10 shows the theoretical curve to be quite conservative.

Additional results obtained from these test data are listed below:

1. The mean of the cycles-to-failure at a stress ratio of  $\infty$  increases as the alternating bending stress level decreases, from about 1900 cycles at a stress level of  $100 \text{ Gg/m}^2$  (150 kpsi) to about 180 000 cycles at a stress level of  $50 \text{ Gg/m}^2$  (70 kpsi).

2. The standard deviation of the cycles-to-failure at a stress ratio of  $\infty$  increases from about 500 cycles at a stress level of  $100 \text{ Gg/m}^2$  (150 kpsi) to about 35 000 cycles at a stress level of  $50 \text{ Gg/m}^2$  (70 kpsi).

3. The endurance strength distribution at a stress ratio of  $\infty$  is best represented by the normal distribution with a mean of  $40 \text{ Gg/m}^2$  (57 kpsi) and a standard deviation of  $0.27 \text{ Gg/m}^2$  (3.8 kpsi).

4. The endurance strength standard deviation at a stress ratio of  $\infty$  is 6.7 percent of the endurance strength mean.

5. The knee of the S-N diagram for a stress ratio of  $\infty$  is at about  $6.0 \times 10^5$  cycles.

6. A comparative study of data for stress ratios of  $\infty$  and 0.83 indicates that there is a significant reduction in the mean fatigue life when the stress ratio is decreased from  $\infty$  to 0.83 by the superimposition of a steady shear stress onto an alternating reversed bending stress. For example, when the stress ratio is reduced from  $\infty$  to 0.83, the mean fatigue life is also reduced by 40 percent at an alternating bending stress level of  $85 \text{ Gg/m}^2$  (120 kpsi) and by 50 percent at an alternating bending stress level of  $49 \text{ Gg/m}^2$  (70 kpsi). At a stress ratio of  $\infty$  and a stress level of  $85 \text{ Gg/m}^2$  (120 kpsi) the mean life is about 7300 cycles.

7. A study of figure 10 reveals that the theoretically constructed S-N diagram for  $r_s = \infty$  and grooved specimens, using Shigley's method (6, p. 162), gives an endurance strength which is 16 percent more conservative than the one determined experimentally, and the mean cycles to failure up to 46 percent more conservative. The start of the theoretical endurance life, however, is 67 percent greater than the experimental.

### CONCLUDING REMARKS

The design, fabrication, development, operation, calibration, and results from reversed bending combined with steady torque fatigue reliability research machines have resulted in useful data from fifteen centimeter long, notched SAE 4340 steel. The test machine developed for this research has advantages which may be useful in other areas:

1. A constant bending moment is maintained by directly applied static loads.
2. Constant torque is maintained through the use of an Infnit-Indexer.
3. Monitoring of the bending moment and the torque is direct through the use of strain gages, slip-rings, and a recorder.

4. Backlash in the four square loop is eliminated by fixed gear engagement.

The cycles-to-failure data for various combinations of stress ratios and bending stresses have been statistically analyzed to develop probabilistic S-N diagrams. These diagrams are used to construct probabilistic modified Goodman diagrams necessary to design specified reliability into rotating components.

#### REFERENCES

1. Mabie, H. H. and Gjesdahl, M. S., "A Fatigue Testing Machine for Reversed Bending and Steady Torque", Proc. SESA, XIV (1), 83-88 (1956).
2. Lalli, V. R. and Kececioglu, D. B., "An Approach to Reliability Determination of a Rotating Component Subject to Complex Fatigue," NASA TM X-52790 (1970).
3. Kececioglu, D. and Smith, J. L., "Statistical Complex Fatigue Data for SAE 4340 Steel and Its Use in Design by Reliability," University of Arizona, NASA CR-72835, 175 (1970).
4. Kececioglu, D. B. and Haugen, E. B., "Interaction Among the Various Phenomena Involved in the Design of Dynamic and Rotary Machinery and Their Effects on Reliability," The University of Arizona, TR 1, 2 and 3, ONR Contract N00014-67-A0209-0002 (1968, 69 and 70).
5. Kececioglu, D. and Cormier, D., "Designing a Specified Reliability Directly Into a Component," Proceedings of the Third Annual SAE-ASME-AIAA Aerospace Reliability and Maintainability Conference, Washington, D.C., 546-565 (1964).
6. Shigley, J. E., Mechanical Engineering Design McGraw-Hill, New York, 631 (1963).

7. Demer, L. J., 'A Review of Observations on the Cracking Characteristics and Fracture of Laboratory Fatigue Specimens,' University of Minnesota, WADC-TN-55-527 (1955).
8. Branger, J., Life Estimation and Prediction of Fighter Aircraft, Smithsonian Institute, Washington, D.C. (1969).
9. Kececioglu, D., Saroni, M. J., Broome, H. W. and McConnell, J., 'Design and Development of and Results from Combined Bending-Torsion Fatigue Reliability Research Machines,' University of Arizona, NASA CR-72838, 57 (1969).
10. Peterson, R. E., Stress Concentration Design Factors, Wiley, New York, 155 (1953).

TABLE I. - OPERATIONAL SPECIFICATIONS FOR THE COMBINED-STRESS  
FATIGUE RESEARCH MACHINES

Test machine <sup>a</sup>	Accomodate a specimen rotating at 1800 rpm; produce and hold a steady torque and a reversed bending moment; holding chuck 2.5 cm diameter maximum; simple design employing "off-the-shell" components.
Loading mechanism for steady torque	Simple device to produce, hold, and transmit desired steady torque of 62 M-kg to test specimen.
Loading mechanism for reversed bending	Simple device to produce a reversed bending moment of 40 kg-M while specimen is rotating.
Test specimen	SAE 4340 steel, Condition C-4; MIL-S-5000B, certification of chemical and physical properties; uniform quality, same heat and processing, heat treat to Rockwell C 35/40 as per MIL-H-6875 with minimum tempering temperature of 538 <sup>0</sup> C; inspection as per MIL-I-6868; D = 1.87 cm, d = 1.27 cm, r = 0.38 cm; K <sub>b</sub> = 1.45; K <sub>s</sub> = 1.22, with 2.5 cm × 0.32 cm keyway.
Instrumentation Strain gages Channels Slip rings Amplifier Recorder	To obtain dynamic and static strain measurements in bending and torsion. To handle at least 6 sets of strain gage outputs simultaneously. To transfer strain gage data to amplifier while specimen is rotating. To amplify static and dynamic output from strain gages. To produce a permanent record of amplified strain gage outputs.

<sup>a</sup>Three such machined have been built to date and are being used to obtain distributional combined stress fatigue data for the steel specimens specified above.

TABLE II. - RESEARCH MACHINE INSTRUMENTATION

Component	Manufacturer	Quantity	Component number	Remarks
Metalfilm strain gages (with leads)	The Budd Co. Instrument Div.	4	324B-190	Bending moment collet
		2	C6-1X1X3X4-ME15E-120	Bending moment groove
Slip rings and brushes	Breeze Corp. Inc.	2	C6-121-R2VC	Torque collet
		1	AJ-8005-A8	Transfer of signals
Amplifier	Honeywell	6	119	Carrier channel, 0-5 KH <sub>Z</sub>
Visicorder		1	906C1	Galvanometer channels 14
Galvanometers		6	M1650	Frequency response 0-5 KH <sub>Z</sub>

TABLE III. - THE CALIBRATION COEFFICIENTS  
FOR EACH RESEARCH MACHINE

Constant <sup>a</sup>	$K_{BGR}$	$K_{GR-TH}$	$K_{T/B}$	$K_T$	$K_{B/T}$
Machine					
1	1.0123	0.0207	-0.0459	0.8752	0.0290
2	1.0123	.0188	.0344	.8200	.0422
3	1.0123	.0198	.0000	.9330	-.0149

<sup>a</sup>Abbreviated constants are explained in the symbols list.

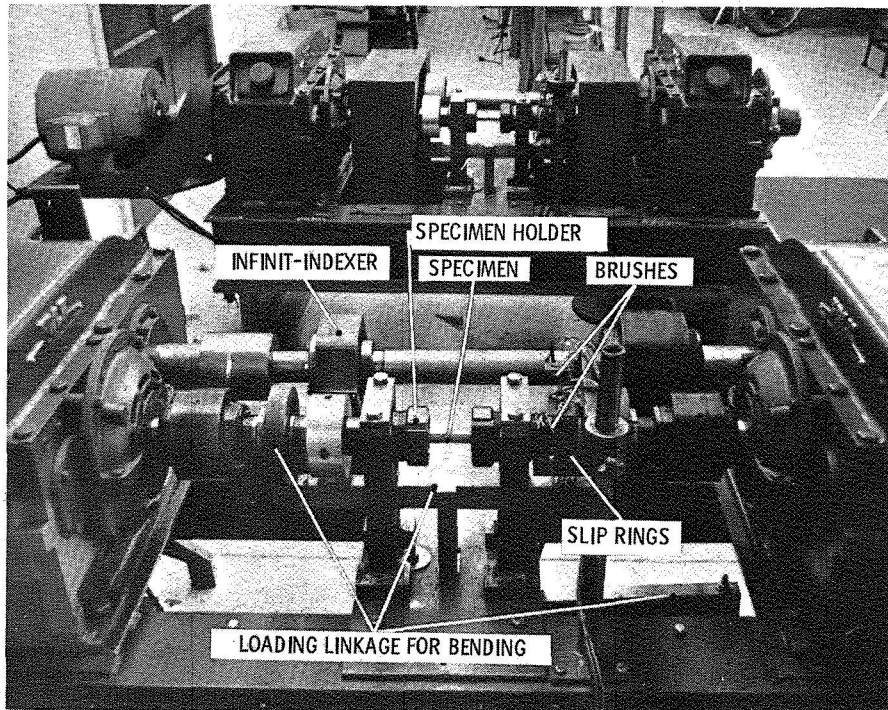
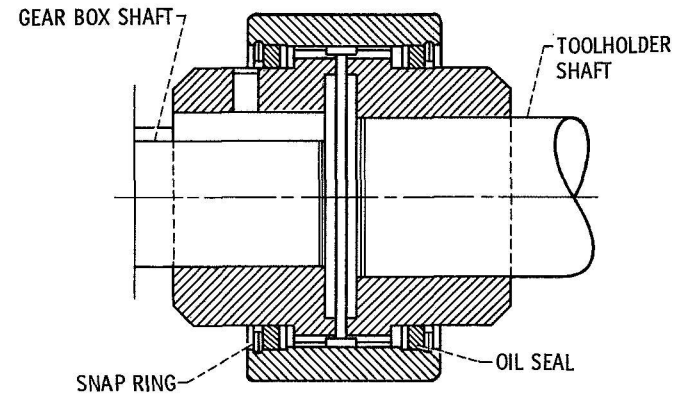
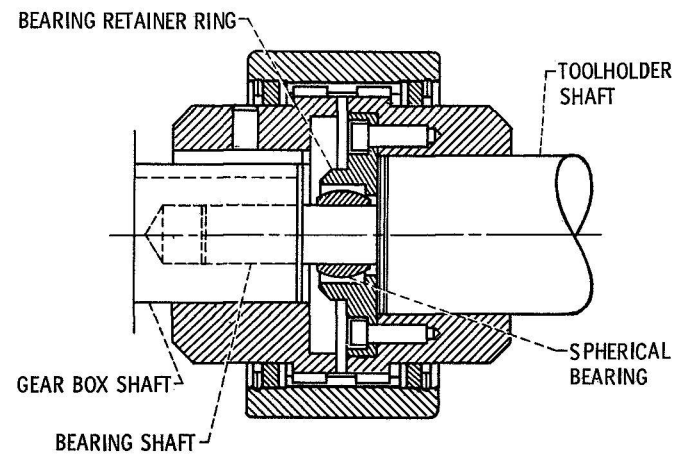


Figure 1. - Close-up of the combined stress fatigue research machine.

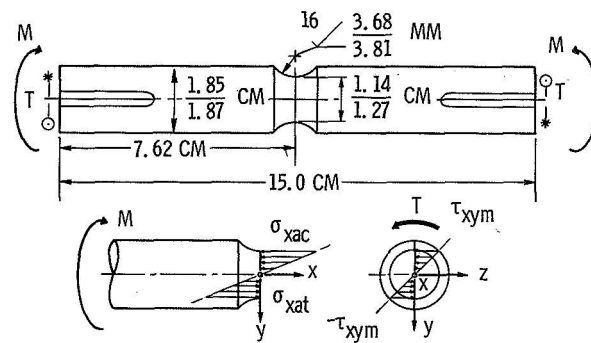


(A) ORIGINAL DESIGN.



(B) FIXED PIVOT POINT DESIGN.

Figure 2. - Front shaft gear coupling design comparison.

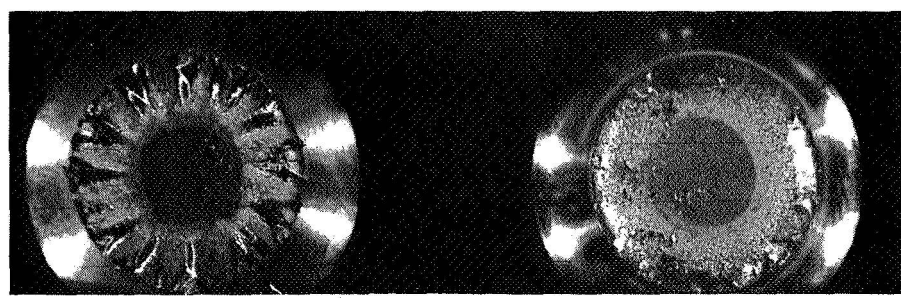


(A) DIMENSIONS, FINISH, FORCES AND STRESSES.

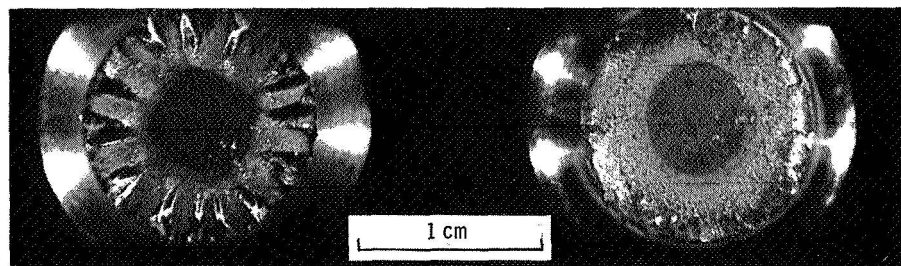


(B) CONFIGURATION BEFORE AND AFTER FATIGUE TESTING.

Figure 3. - Test specimen details.



The crack starts at the surface of the groove, and grows toward the center causing the specimen to fracture as shown in these two test specimens.



(a)  $\bar{r}_s = 0.83; \bar{\sigma}_{xa} = 78.0 \text{ Gg/m}^2$ .

(b)  $\bar{r}_s = \infty; \bar{\sigma}_{xa} = 80.0 \text{ Gg/m}^2$ .

Figure 4. - Close-up view of fractured section at the notch.

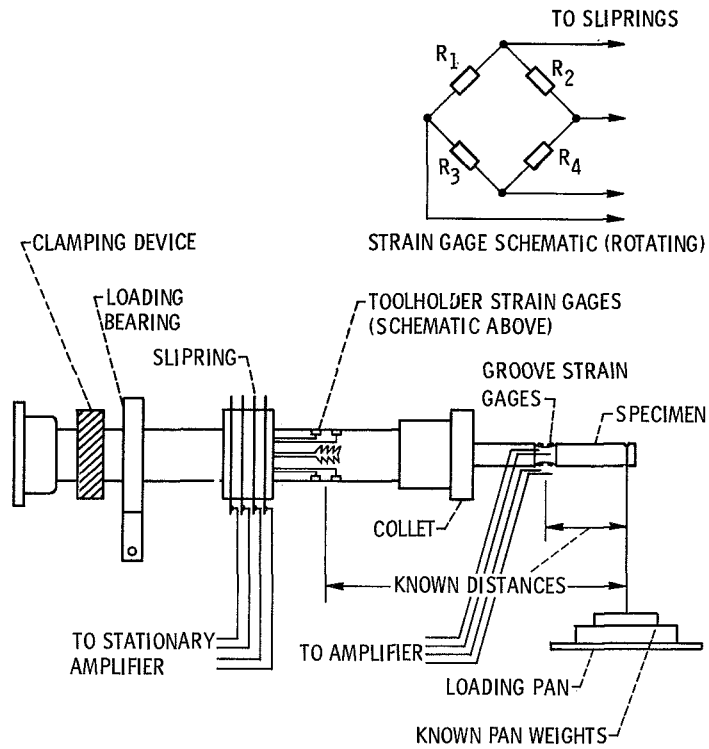
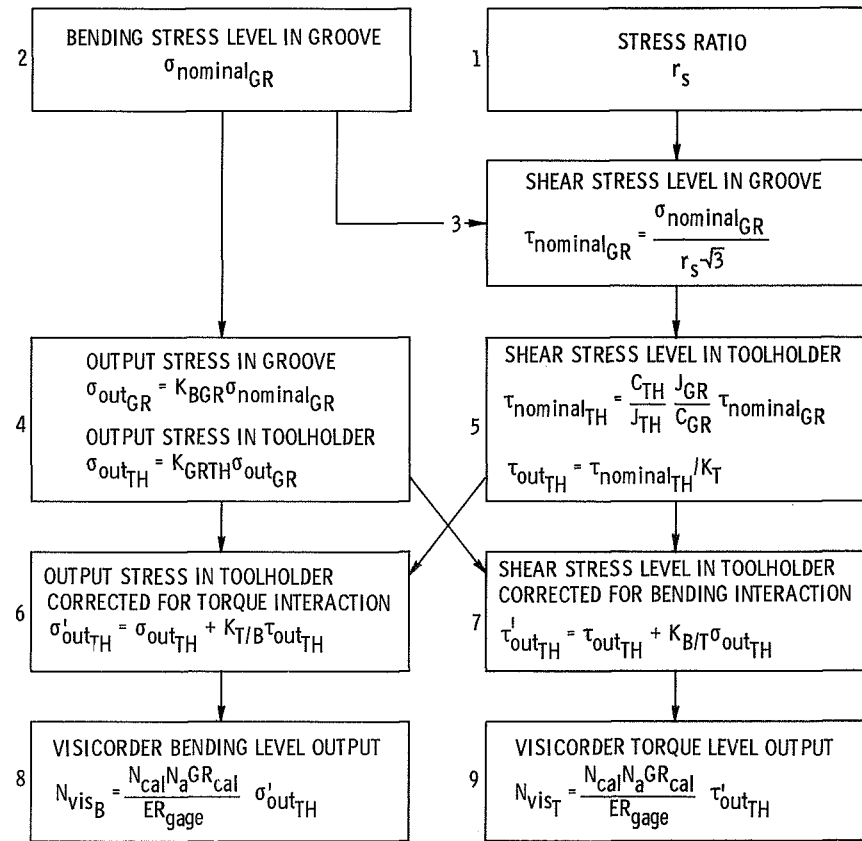


Figure 5. - Test setup for bending calibration.



NOTE: THIS CHART SHOWS THE MODE OF USE OF THE CALIBRATION RESULTS GIVEN IN TABLE III TO ASSURE PROPER SPECIMEN ENVIRONMENT. A PLANNED TASK FOR PHASE II IS TO MONITOR SPECIMEN ENVIRONMENTAL PARAMETERS WITH AN ANALOG COMPUTER SET WITH LIMITS TO REDUCE OUT-OF-TOLERANCE TESTING TO LESS THAN 5 PERCENT.

Figure 6. - Calibration flow chart.

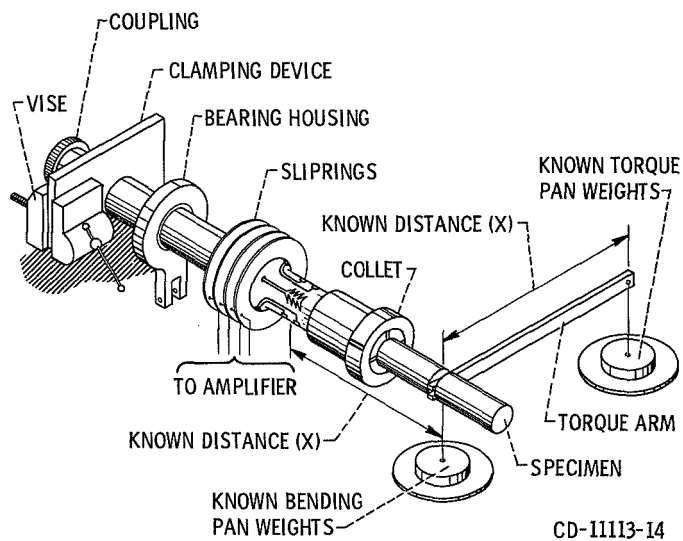


Figure 7. - Test setup for torque calibration.

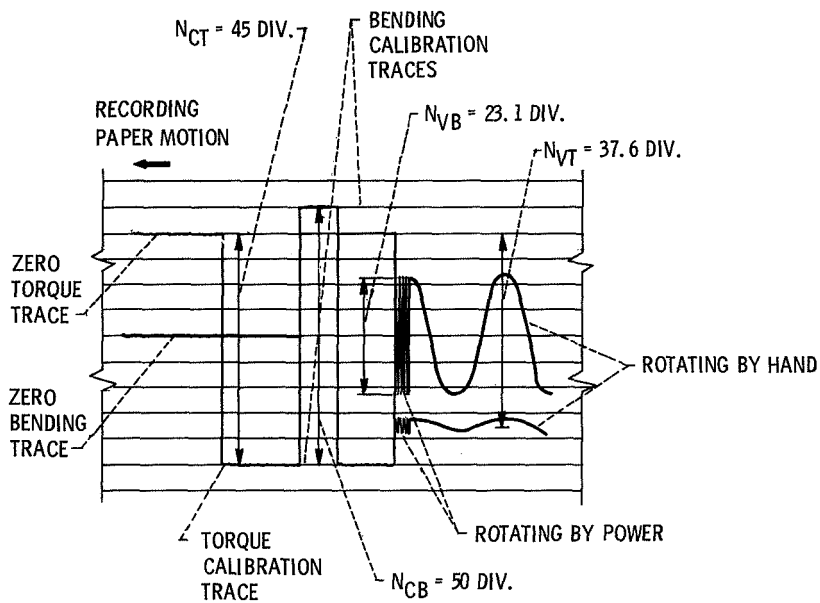


Figure 8. - Recording illustration of torque and bending gage signals.

L-6580

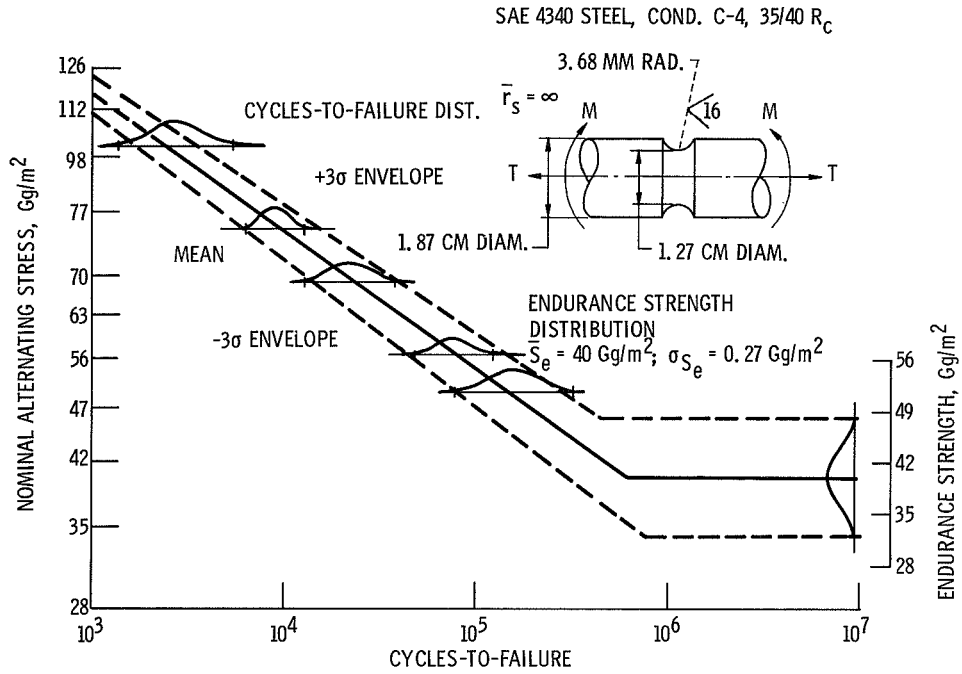


Figure 9. - Probabilistic S-N diagram.

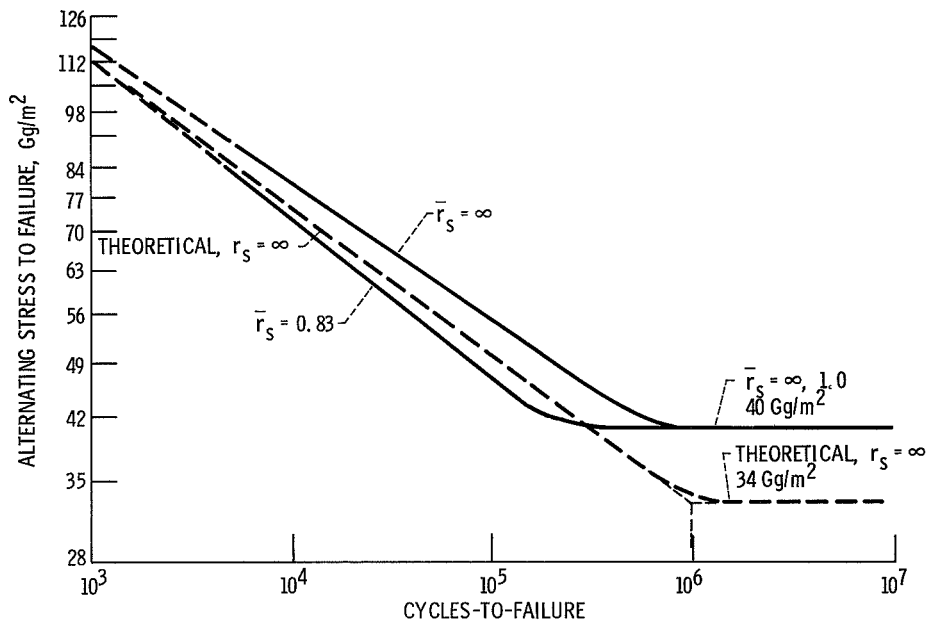


Figure 10. - Mean value S-N diagram comparison -  $r_s$  of  $\infty$ , 0.83 and 1.0.